Impact of single-site axonal GABAergic synaptic events on cerebellar interneuron activity

Javier Zorrilla de San Martin, Abdelali Jalil, and Federico F. Trigo

Laboratoire de Physiologie Cérébrale, Université Paris Descartes and Centre National de la Recherche Scientifique, CNRS UMR8118, 75794 Paris, France

Axonal ionotropic receptors are present in a variety of neuronal types, and their function has largely been associated with the modulation of axonal activity and synaptic release. It is usually assumed that activation of axonal $GABA_A$Rs comes from spillover, but in cerebellar molecular layer interneurons (MLIs) the GABA source is different: in these cells, GABA release activates presynaptic $GABA_A$ autoreceptors (autoRs) together with postsynaptic targets, producing an autoR-mediated synaptic event. The frequency of presynaptic, autoR-mediated miniature currents is twice that of their somatodendritic counterparts, suggesting that autoR-mediated responses have an important effect on interneuron activity. Here, we used local Ca^{2+} photolysis in MLI axons of juvenile rats to evoke GABA release from individual varicosities to study the activation of axonal autoRs in single release sites. Our data show that single-site autoR conductances are similar to postsynaptic dendritic conductances. In conditions of high $[Cl^-]_i$, autoR-mediated conductances range from 1 to 5 nS; this corresponds to ∼30–150 $GABA_A$ channels per presynaptic varicosity, a value close to the number of channels in postsynaptic densities. Voltage responses produced by the activation of autoRs in single varicosities are amplified by a Na_v-dependent mechanism and propagate along the axon with a length constant of 91 µm. Immunolabeling determination of synapse location shows that on average, one third of the synapses produce autoR-mediated signals that are large enough to reach the axon initial segment. Finally, we show that single-site activation of presynaptic $GABA_A$ autoRs leads to an increase in MLI excitability and thus conveys a strong feedback signal that contributes to spiking activity.

INTRODUCTION

The recognition that ionotropic receptors, and specifically $GABA_A$ receptors, occur in the axonal compartment of neurons dates back to two studies in the early 1960s, one by Eccles et al. (1962) in the cat spinal cord and the other by Dudel and Kuffler (1961) in the crayfish neuromuscular junction. Since these classical papers, axonal $GABA_A$ receptors have been described in a variety of preparations, both in the central and peripheral nervous system. Although various functions have been ascribed to them, including modulation of spiking activity, action potential (AP) transmission, and transmitter release (Kullmann et al., 2005; Trigo et al., 2008; Ruiz and Kullmann, 2012), much remains to be learned about their physiological role.

Molecular layer interneurons (MLIs) of the juvenile cerebellar cortex are known to possess axonal $GABA_A$Rs (Pouzat and Marty, 1999). When an AP is induced in the soma of an MLI, GABA is released from multiple axonal varicosities; the released GABA binds to synaptic $GABA_A$Rs in the somatodendritic domain of the postsynaptic cell, producing a prototypical GABAergic postsynaptic current. Concomitantly, the released GABA also binds to presynaptic, or axonal, $GABA_A$Rs, producing an autoreceptor (autoR) current that backpropagates to the soma. AutoR currents can be distinguished from autaptic currents by their slower kinetics and different developmental expression (Pouzat and Marty, 1999, 1998). In summary, in MLIs the same GABA transient in the synaptic cleft is able to activate $GABA_A$Rs located in both the post- and the presynaptic membranes and hence produces both a postsynaptic event and an autocrine, presynaptic event.

It was recently shown that autoRs can be activated by spontaneous, spike-independent release of GABA. This quantal activation of the autoRs produces a type of miniature event that can be recorded from the soma and was called "premini" (from "presynaptic autoR-mediated miniature current"; Trigo et al., 2010). Preminis represent the activation of autoRs by the GABA released from spontaneous vesicular fusion events. Surprisingly, the frequency of preminis is higher than that of classical,

Correspondence to Federico F. Trigo: federico.trigo@parisdescartes.fr

Abbreviations used in this paper: AIS, axon initial segment; AP, action potential; ASC, autoreceptor-mediated synaptic current; ASP, autoreceptor-mediated synaptic potential; autoR, autoreceptor; DM-nitrophen, 1-(2-nitro-4,5-dimethoxyphenyl)-*N*,*N*,*N*′,*N*′-tetrakis[(oxycarbonyl)methyl]-1,2-ethanediamine; DPNI-GABA, 1-(4-aminobutanoyl)-4-[1,3-*bis*(dihydroxy-phosphoryloxy)propan-2-yloxy]-7-nitroindoline; Gbz, gabazine; IS, internal solution; MLI, molecular layer interneuron; RRS, readily releasable pool; TTX, tetrodotoxin; VGAT, vesicular GABA/glycine transporter.

The Rockefeller University Press $30.00
J. Gen. Physiol. Vol. 146 No. 6 477–493
www.jgp.org/cgi/doi/10.1085/jgp.201511506

postsynaptic, somatodendritic miniature events and is modulated by subthreshold membrane fluctuations in the somatodendritic compartment (a type of analogue signaling: somatic depolarizations increase premini frequency and somatic hyperpolarizations decrease it; Trigo et al., 2010). Although the role of the AP-dependent activation of axonal autoRs has already been addressed (Mejia-Gervacio and Marty, 2006), the impact of spontaneous miniature axonal synaptic events remains unknown. Understanding the physiological role and the mechanisms of action of these miniature events is extremely important: in electrically compact cells like MLIs, individual somatodendritic quantal events strongly affect spiking behavior (Carter and Regehr, 2002), suggesting that axonal preminis could also make an important contribution to the cell's activity.

To elucidate the role of AP-independent, autoR-mediated synaptic events and to study the biophysical mechanisms that mediate their propagation along the axon, it is necessary to evoke the release of GABA at individual synapses in specific axonal locations. To address this issue, we developed a new approach to the study of autoRs that consists in eliciting GABA release in single identified varicosities using local calcium photolysis. This, in combination with electrophysiology, modeling, and immunohistochemistry, allowed us to provide the first quantitative description of the autoR-mediated currents and filtering of axonal synaptic events. In voltage clamp, AutoR-mediated currents displayed a marked site-to-site heterogeneity, probably reflecting variations in numbers of $GABA_A$Rs among sites, as well as degrees of attenuation that varied accordingly to the distance of each site to the soma. In current clamp, autoR-mediated somatic signals were surprisingly large. When using physiological intracellular Cl^- concentration, single-site autoR-mediated depolarizations reached several millivolts and were enhanced by activation of axonal voltage-dependent Na^+ channels. Finally, autoR-mediated depolarizations cooperated with short somatic current injections mimicking somatodendritic excitatory postsynaptic currents over periods of time reaching several hundreds of milliseconds, often resulting in AP firing.

MATERIALS AND METHODS

General procedures

11–14-d-old Sprague Dawley rats (either male or female) were used to prepare sagittal cerebellar slices following institutional guidelines. In brief, the animal was placed under deep anesthesia using isoflurane and decapitated. The cerebellar vermis was quickly removed. 200-µm-thick parasagittal slices were cut with a vibroslicer (VT1200S; Leica) in an ice-cold artificial cerebrospinal fluid and then placed in an incubating chamber for 60 min at 34°C. Thereafter, slices were kept at room temperature. The same bicarbonate-buffered saline was used as the cutting and storing solution. The composition was (mM): 115 NaCl, 2.5 KCl, 26 $NaHCO_3$, 1.3 NaH_2PO_4, 25 glucose, 2 $CaCl_2$, 1 $MgCl_2$, 5 Na-pyruvate, with osmolality adjusted to 300 mOsm kg^{-1} H_2O and pH set at 7.4 by the continuous bubbling of a mixture of 5% CO_2 and 95% O_2.

Electrophysiology

MLIs were visualized under a microscope with a 63×/0.9-NA water-dipping objective (Axio Scope; Carl Zeiss) and recorded with the patch technique under the whole-cell configuration, both in voltage and current clamp, with an amplifier (EPC 10; HEKA). The composition of the internal solution (IS) used for the high $[Cl^-]_i$ experiments was as follows (mM): 90 KCl, 50 HEPES, 0.5 $MgCl_2$, 4.25 $CaCl_2$, 5 Na_2ATP, 20 NaCl, 0.5 NaGTP, 25 KOH, 5 1-(2-nitro-4,5-dimethoxyphenyl)-*N*,*N*,*N*′,*N*′-tetrakis[(oxycarbonyl)methyl]-1,2-ethanediamine (DM-nitrophen), 0.08 Alexa Fluor 488 (or 594 for the experiments in Fig. 1, A and B), and 10 GABA (to avoid washout of intracellular GABA; Bouhours et al., 2011). KCl was replaced by 110 or 100 mM K-gluconate for the experiments with $[Cl^-]_i$ = 15 and 25 mM, respectively. IS had a pH of 7.3 and an osmolality of ≈300 mOsm kg^{-1} H_2O. Recordings were made at room temperature (22–24°C). In the experiments performed with the low $[Cl^-]_i$ IS (Figs. 5–7), the membrane potential was corrected for a 12-mV liquid junction potential value (calculated with Patcher's Power Tools for Igor Pro; F. Mendez and F. Würriehausen, Max-Planck-Institut Für Biophysikalische Chemie, 37077 Göttingen, Germany). Pipette resistance was ∼5 MΩ when filled with the high $[Cl^-]_i$ IS and ∼10 MΩ when filled with the low $[Cl^-]_i$ IS. Series resistance was compensated by 50%. Recordings with SR higher than 25 MΩ were discarded. Holding potentials were usually −60 mV. MLI identification was confirmed by the observation of large (0.8–1.7-nA), unclamped Na^+ currents when the membrane potential was stepped from −60 to 0 mV for 2 ms (Pouzat and Marty, 1999). Recordings were filtered at 5 kHz with a Bessel filter. Data were analyzed using routines written in Igor Pro (WaveMetrics). Most data were obtained from cells located in the proximal part of the molecular layer (basket cells); however, interneurons located in the distal molecular layer (stellate cells) were also included. Reagents were purchased from Sigma-Aldrich, and gabazine (Gbz) and tetrodotoxin (TTX) were from Abcam.

Photolysis

Photolysis of DM-nitrophen. Photolysis of DM-nitrophen (Kaplan and Ellis-Davies, 1988) was implemented at 405 nm. Light from a diode laser (DeepStar 405; Omicron) was focused through the 63× Zeiss objective as an ∼2-µm diameter spot in the objective focal plane. Laser pulse duration was 100 µs, and laser power was between 1 and 2.5 mW under the objective. The calibration of laser photolysis and additional details are given elsewhere (Trigo et al., 2009a). Lyophilized DM-nitrophen (Synaptic Systems) was dissolved in KOH solution in a 1:4 (DM-nitrophen/K^+) proportion and stored at −20°C. The potassium salt was then added to the intracellular solution the same day of the experiment.

Illumination of the varicosity of a DM-nitrophen–loaded MLI with one laser pulse (duration: 100 µs, 0.2 µJ) produces an increase of $[Ca^{2+}]_i$ of ∼15 µM. This laser energy is enough to trigger the release of all the vesicles that are part of the readily releasable pool (RRP; Trigo et al., 2012).

Upon photolysis of DM-nitrophen, two net OH ions are formed per molecule of Ca^{2+} DM-nitrophen photolyzed. To buffer this pH change, 50 mM HEPES was used (see composition of IS above). Even with this high HEPES concentration, a pH change of ≈0.37 pH units is expected; in similar experimental conditions, this pH change had no effect on synaptic transmission (Trigo et al., 2012). The number of repetitions that can be performed when intracellularly photolyzing DM-nitrophen is limited. In this work, the maximum number of repetitions were 12 and 22 with high and low $[Cl^-]_i$ solutions, respectively. This is not caused by direct photodamage with the 405-nm laser because it is not observed when photolyzing other caged compounds in the extracellular

milieu, like glutamate or GABA, with the same method (Trigo et al., 2009b; this work, Fig. 8); rather, it may be caused by the release of oxidizing subproducts (nitrosoacetophenone; Kaplan and Ellis-Davies, 1988), but the exact mechanisms remain to be explored.

Photolysis of GABA. GABA was released from 1-(4-aminobutanoyl)-4-[1,3-*bis*(dihydroxy-phosphoryloxy)propan-2-yloxy]-7-nitroindoline (DPNI-GABA) with the same 405-nm laser as that used for the photolysis of DM-nitrophen. DPNI-GABA was purchased from Tocris Bioscience and prepared as 25-mM stocks in a HEPES-buffered NaCl solution, with osmolality of 300 mOsm/KgH_2O and pH 7.0. Photolysis was performed in a HEPES-buffered saline, with the following composition (mM): 128 NaCl, 4 KCl, 2.5 $NaHCO_3$, 10 HEPES, 25 glucose, 5 Na-pyruvate, 2 $CaCl_2$, and 1 $MgCl_2$, with pH 7.4 adjusted with NaOH 1N and osmolality of 300 mOsm kg^{-1} H_2O. Once the axon of the cell became clearly distinguishable with fluorescence, the perfusion was turned off to minimize the usage of the drug and DPNI-GABA was added directly to the bath. The final concentration of DPNI-GABA was quantified by spectrophotometry with a NanoDrop 1000 (Thermo Fisher Scientific); the absorption coefficient used to calculate the concentration was 4,229 M^{-1} cm^{-1} at 355 nm (Trigo et al., 2009b). Bath concentrations of DPNI-GABA ranged from 0.62 to 1.89 mM; the mean was 1.37 ± 0.16 mM (mean ± SEM; n = 10 samples). Photolysis was performed at least 5 min after the addition of the drug to allow equilibration in the solution; the duration of laser pulse was between 0.3 and 1 ms, and the power was between 1 and 2.5 mW under the objective.

Fluorescence imaging

Epifluorescence excitation was by light-emitting diode in a dual–lamp house controlled by an OptoLED system (Cairn Research) at 470-/40-nm (and 572-/35-nm; Fig. 1, A and B) excitation; fluorescence emitted at 520/40 nm (and 630/60 nm; Fig. 1, A and B) was detected with an electron-multiplying CCD camera (Andor Technology; filters from Chroma Technology Corp.). The second channel of the lamp house was used to connect the optic fiber coming from the photolysis laser. After each experiment, a series of epifluorescence images was taken to perform morphological reconstructions and to measure the distance between the release sites and the soma. ImageJ (National Institutes of Health) was used to make the stacks and composite images.

Neuron simulations

The NEURON simulation environment (Hines and Carnevale, 1997) was used to model MLIs and their axonal synaptic inputs. Values for the biophysical parameters included in the model were taken from previously validated models (Pouzat and Marty, 1999; Mejia-Gervacio et al., 2007). The model comprised two connected, cylindrical compartments: one corresponding to the soma and dendrites (10-µm length × 10-µm diameter), and the other one to the axon (200-µm length × 0.5-µm diameter). The parameters used for the NEURON model are listed next. Somatodendritic compartment: cytoplasmic resistivity, Ra = 35.4 Ω/cm; Cm = 1 µF/cm^2; g_pas = 2×10^{-5} S/cm^2; e_pas = −70 mV; axonal compartment: Ra = 100 Ω/cm; membrane capacitance: Cm = 1 µF/cm^2; total passive conductance: g_pas = 2×10^{-5} S/cm^2; total passive conductance reversal potential: e_pas = −70 mV; voltage-dependent sodium conductance density: gNabar_hh = 0.05 S/cm^2; voltage-dependent potassium conductance density: gKbar = 0.4 S/cm^2; sodium reversal potential: eNa = 50 mV; potassium reversal potential: eK = −75 mV; synaptic input: alpha synapse; tau = 3 ms; synaptic conductance was left as a free variable to estimate its value. Axonal synaptic inputs at different positions were simulated to observe the impact of axonal filtering on the amplitude of synaptic currents recorded from the soma. The procedure was iteratively repeated over a range of synaptic conductance values. Goodness of fit of simulated to experimental datasets was tested with the Chi^2 test.

Slice fixation, immunofluorescence, and 3-D image analysis

Quantification of the number of varicosities in a neuron has proven to be a complicated task, mainly because of the inability to unequivocally assign a labeled site to a given neuron. To tackle this problem, we combined 3-D reconstruction of Alexa Fluor 488–filled MLIs with post-hoc immunolabeling of GABAergic varicosities using antibodies against the vesicular GABA/glycine transporter (VGAT), similar to what was reported by Fogarty et al. (2013). To label MLIs, Alexa Fluor 488 was included in the intracellular solution used for whole-cell patch-clamp recordings. Several minutes after break-in, the recording pipette was pulled out and the slice was fixed in 0.01 M PBS and 4% PFA for 30 min, and then rinsed with 0.01 M PBS. The slices were incubated in PBS containing 0.3% Triton X-100 and 10% fetal bovine serum for 5 h at room temperature, and then at 4°C overnight with a mouse monoclonal antibody anti-VGAT (Synaptic Systems) diluted to 1/500 in PBS containing 1 mg/ml BSA. After three washes in PBS, the slices were incubated for 3 h with secondary goat anti–mouse IgG conjugated to Alexa Fluor 647 (Molecular Probes) diluted to 1/500 in PBS-BSA buffer. Slices were then washed and mounted between slide and coverslip using mounting medium (Fluoromont G; SouthernBiotech). Tiles of image stacks were acquired using an upright confocal microscope (LSM 710; Carl Zeiss) equipped with 63× Plan-Apochromat 63×/1.4 NA oil-objective and appropriate lasers (argon 488 and helium-neon 633 nm) and emission filters (BP 505–530 and LP 650).

For a detailed description of the morphology of MLIs, the recovered cells were reconstructed using semi-automated methods implemented in Vaa3D software (Peng et al., 2010). The intensity profiles of the Alexa Fluor and VGAT signals corresponding to the voxels contained in the 3-D reconstruction were exported to be analyzed in Igor Pro. In some segments, a clear baseline was observed, normally in the initial part of the axon. These segments were used to define the intensity baseline for each reconstructed axon; otherwise, baseline was taken from segments without any VGAT labeling chosen by eye. The VGAT-labeling intensity threshold to detect a GABA varicosity was set at baseline +2 standard deviations. Furthermore, to avoid detection of spurious sites, a second criterion was used: supra-threshold intensity spots that occupied <500 linear nanometers in the longitudinal direction were also discarded.

Statistical analysis

Statistical differences between experiments were assessed with Student's t test or Kruskal–Wallis test, as appropriate. Normality of datasets was tested with the D'Agostino–Pearson test. In all cases, $P < 0.05$ was considered significant. Correlations were evaluated with Pearson's coefficient. Kinetic parameters of autoR-mediated synaptic currents (ASCs) were measured on the average traces obtained from all the repetitions obtained from an individual release site. τ_{rise} and τ_{decay} were estimated by fitting each of the phases with a mono-exponential function. Data are presented as mean ± SEM unless otherwise stated.

RESULTS

Local caged-Ca^{2+} photolysis evokes ASCs from single release sites

In young MLIs, axonal varicosities are both the source and the target of GABAergic signaling. This makes the disentangling of the causal sequences of the events following the activation of axonal $GABA_A$ receptors particularly

difficult. To separate pre- from postsynaptic mechanisms, we combined electrophysiological recordings with laser calcium photolysis in individual varicosities. Uncaging with a minimized laser spot allowed us to induce GABA release with a high spatial resolution and therefore to characterize the signals evoked from a single varicosity. We first designed experiments to assess the feasibility of using laser photolysis of Ca^{2+} to record autoR-mediated single-site responses in MLIs. To do this, we recorded two putative connected MLIs with a high chloride IS. The IS of the presynaptic cell also contained the calcium cage DM-nitrophen and Alexa Fluor 594; the IS of the postsynaptic cell contained Alexa Fluor 488. The fluorescent dyes were included for neurite identification. Because of the advantageous morphology of juvenile MLIs, which display a planar orientation along the parasagittal plane, direct online inspection under the microscope a few minutes after break-in readily distinguishes dendrites, which are thick and short, from the axon, which is thinner and longer and can be followed up to a few hundred micrometers (Trigo et al., 2012). When a putative synaptic contact (black arrowhead in Fig. 1 A, right) between the presynaptic axon (in green) and the postsynaptic dendrite (in magenta) was localized under LED excitation, we focused the 405-nm laser and photolyzed DM-nitrophen (see Trigo et al., 2012). Photolysis of DM-nitrophen induces a fast and homogeneous calcium transient in the presynaptic varicosity and, subsequently, a fast postsynaptic current (Fig. 1 B, bottom) that can be blocked by $GABA_A$Rs antagonists (not depicted). As predicted from previous work (Pouzat and Marty, 1999; Trigo et al., 2010), concomitantly to the postsynaptic current we recorded a presynaptic current that has a smaller amplitude and a longer rise time (Fig. 1, B, top, and C), very similar to the spontaneous axonal miniature synaptic currents (preminis) described previously (Trigo et al., 2010). It is unlikely that the evoked currents represent spillover of GABA because previous EM experiments have shown that presynaptic $GABA_A$Rs are located in the synapse (Trigo et al., 2010). In the pair shown in Fig. 1 (A and B), the latency to the beginning of the presynaptic current is virtually the same as the latency to the postsynaptic current (1.6 ms). The pre- and postsynaptic average latencies in the four recorded pairs are shown in Fig. 2 C (left), the pre- and postsynaptic average τ_{rise} are shown in Fig. 1 C (middle), and the pre- and postsynaptic average amplitudes are shown in Fig. 1 C (right).

The next series of experiments was designed to characterize the autoR-mediated synaptic events. To do this,

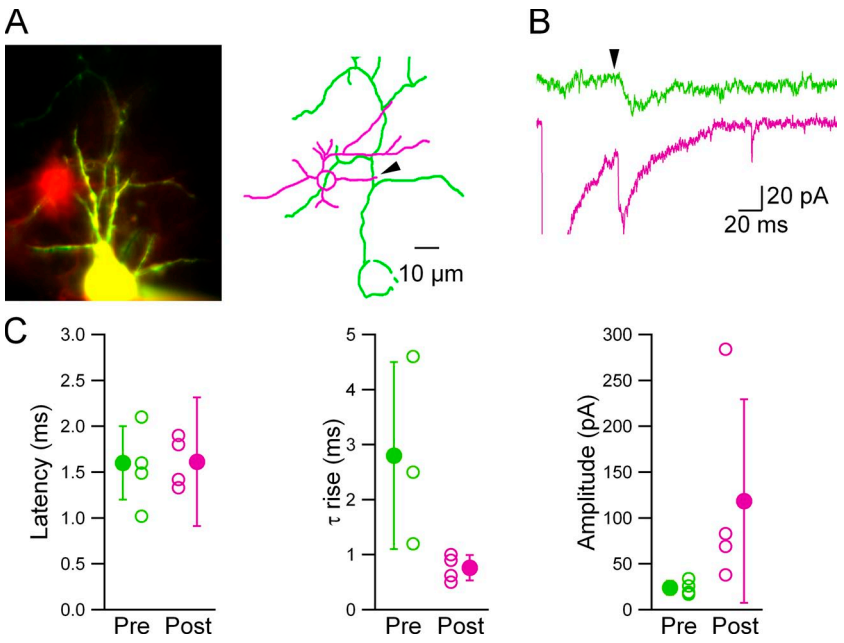

Figure 1. Laser photolysis of caged Ca^{2+} in axonal varicosities between two connected MLIs evokes simultaneous pre- and postsynaptic currents. (A; left) Fluorescence picture taken with a CCD camera. (Right) Reconstruction of a pair of synaptically connected MLIs. The presynaptic cell is shown in green, and the postsynaptic cell is in magenta. The stimulated site is indicated with the arrowhead in the reconstruction. (B) Simultaneous pre- (top, green) and postsynaptic (bottom, magenta) currents recorded when photolyzing DM-nitrophen with a 100-µs laser pulse. The recordings correspond to individual traces. (C) Latency (left), τ_{rise} (middle), and amplitude (right) of pre- (green symbols) and post- (magenta symbols) synaptic currents recorded simultaneously in four different pairs. Open circles correspond to individual experiments, and closed circles correspond to the averages ± SD. Average ± SD values are: pre- and postsynaptic latencies: 1.6 ± 0.4 and 1.6 ± 0.2 ms, respectively; pre- and postsynaptic τ_{rise}: 2.8 ± 1.7 and 0.8 ± 0.2 ms, respectively ($n = 3$ for the presynaptic measurements caused by the difficulties in measuring the τ_{rise} in one of the recordings); and pre- and postsynaptic amplitudes: 24 ± 7.7 and 118.5 ± 111 pA, respectively.

we only recorded from the presynaptic cell. As in the previous set of experiments, somatic whole-cell recordings were performed with an intracellular solution containing Alexa Fluor 488, the Ca^{2+} cage DM-nitrophen, and high $[Cl^-]_i$ to maximize the driving force for $GABA_A$ receptors (E_{GABA} = 3 mV). Fig. 2 A shows the somatodendritic compartment and the proximal part of the axon of an Alexa Fluor–filled MLI. Scattered along the axon, it is possible to observe many elongated bright spots, or varicosities (Fig. 2 A, inset; see also Fig. 3 C), that correspond to GABA release sites (Llano et al., 1997; Forti et al., 2000; Rowan et al., 2014; Trigo et al., 2012). As in the paired experiment of Fig. 1, when the minimized laser spot (λ = 405 nm) was focused onto such an axonal varicosity, photolysis of caged Ca^{2+} with 100-µs pulses evoked inward currents, as recorded from the soma of the cell (Fig. 2 B; black traces are individual sweeps, and the gray trace is the average). Again, these inward currents closely resembled preminis; here, we call them ASCs (autoR-mediated synaptic currents) because, contrary to preminis, they mainly involve multi-vesicular release. In the cell shown in Fig. 2 A, photolysis was repeated seven times in the same varicosity, located at 54 µm from the center of the soma; the average amplitude of the responses was 26 ± 1 pA; its τ_{rise} was 3.1 ± 0.9 ms, its τ_{decay} was 76.0 ± 3.4 ms, and the average latency from the laser pulse was 1.06 ± 0.23 ms. When inspecting the expanded traces, it can be observed that some of the events show multiple peaks (black circles in Fig. 2, B and G); these correspond to multiple vesicular release events, as was already described when the same approach was used to study postsynaptic currents in MLI pairs (Trigo et al., 2012).

The addition of the specific $GABA_AR$ antagonist SR 95531 (Gbz) to the bath reversibly blocked the laser-evoked ASCs (Fig. 2 C shows representative traces of individual ASCs, and Fig. 2 D shows summarized data), confirming that ASCs are mediated by $GABA_A$Rs. To

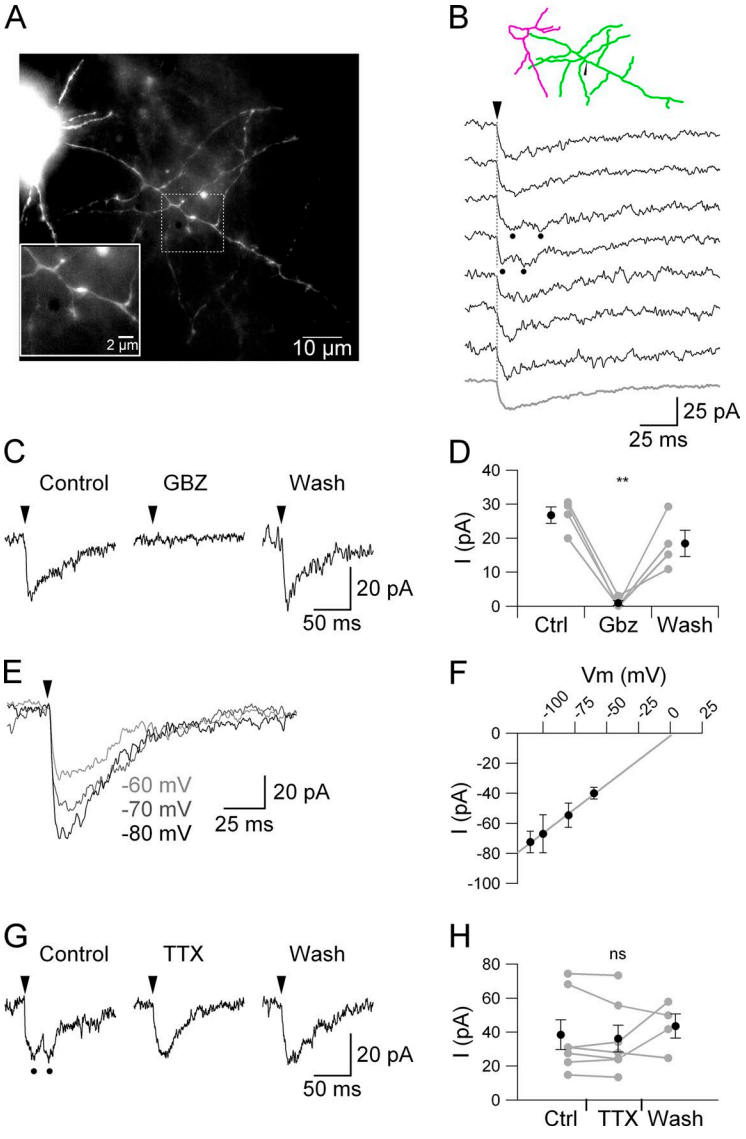

Figure 2. Laser photolysis of caged Ca^{2+} in MLI axonal varicosities evokes ASCs. (A) MLI loaded with an intracellular solution containing Alexa Fluor 488 and the Ca^{2+} cage DM-nitrophen. The image corresponds to a Z projection of a stack of epifluorescence images taken at 1-µm steps. (Inset) Detail of the axon centered on the varicosity where the 405-nm laser was focused. (B) The top part of the panel corresponds to a drawing of the cell; the somatodendritic compartment is shown in magenta, and the axonal compartment is in green. The stimulated site is indicated with the arrowhead. Somatic whole-cell recordings of the laser-evoked ASCs recorded when the varicosity shown in A (inset) was stimulated. Black traces are individual sweeps; the gray trace is the average. Black dots in B and G indicate probable multi-vesicular release events. (C) The specific $GABA_AR$ antagonist, Gbz, completely blocked the laser-evoked ASCs. Representative traces of laser-evoked ASCs in control condition, during Gbz, and after 5-min wash. (D) Summary plot of the effect of Gbz (control: 27 ± 2 pA; Gbz: 1 pA ± 1 pA; after wash: 18 ± 8 pA; one-way ANOVA; **, P < 0.01; *n* = 4 sites). (E) Voltage dependence of ASCs is consistent with $GABA_AR$-mediated currents. Representative traces of ASCs evoked at different holding potentials. (F) The extrapolated ASC reversal potential is not different from the E_{GABA} predicted by the Goldman–Hodgkin–Katz equation. Continuous line, linear fit. Circles represent mean ± SEM. The extrapolated reversal potential is 2 ± 2 mV. (G) Block of Na_v channels failed to affect laser-evoked ASCs. Representative traces of laser-evoked ASCs in control condition, during TTX, and after 5-min wash. (H) Summary plot of the effect of TTX on laser-evoked ASCs (control: 39 ± 9; in 1 µM TTX: 36 ± 8 pA; after wash: 44 ± 14 pA; one-way ANOVA; P > 0.05, *n* = 7 sites). In D and H, the black circles represent mean ± SEM for each condition, and gray dots represent the average amplitude of events evoked in individual release sites. In B, C, E, and G, arrows represent timing of the laser pulse.

further study the identity of the laser-evoked conductance, we estimated the reversal potential of the ASCs by measuring the responses at different holding potentials (Fig. 2, E and F). The resulting reversal potential (2 ± 2 mV; $n = 5$ sites), calculated by extrapolation of the linear fit to the data points, was not different from the E_{GABA} estimated by the Goldman–Hodgkin–Katz equation ($E_{GABA} = 3$ mV). The conductances estimated from the slopes of ASC I-V curves ranged from 0.6 to 2.8 nS per synapse (1.14 ± 0.42; mean ± SEM). To eliminate the influence of other neurons releasing GABA onto the patched cell, we recorded the laser-evoked ASCs in the presence of the voltage-dependent Na^+ channel (Na_v) blocker, TTX. To monitor the time course of TTX action, we evoked somatic Na_v currents with depolarizing steps before, during, and after application of the drug (not depicted). Bath application of TTX failed to produce any significant change in the amplitude of the laser-evoked ASCs (Fig. 2 G for representative traces and Fig. 2 H for summarized data). Finally, consistent with a specific localization of the neurotransmitter release machinery in presynaptic specializations, caged-Ca^{2+} photolysis in dendritic postsynaptic varicosities failed to produce any current (not depicted). Collectively, the experiments presented so far show that the calcium photolysis approach can be used to evoke autoR-mediated responses in presynaptic varicosities of MLIs. This is extremely relevant for the study of the physiology of $GABA_A$ autoRs. Because photolysis of caged Ca^{2+} induces vesicular GABA release, the method produces a more realistic activation of the receptors in terms of concentration and time course of the agonist in the synaptic cleft compared with other agonist application methods (iontophoresis, puff application).

Local caged-Ca^{2+} photolysis evokes ASCs with single release-site resolution

To estimate the spatial resolution of the system, we first measured the point-spread function of the laser spot (see Materials and methods). Fig. 3 shows the distribution of the light intensity near the focus, both in the horizontal (A) and axial (B) coordinates; the $1/e^2$ values, taken from the fits of the experimental data points with Gaussian functions (Fig. 3, A and B, bottom), were 1.4 µm for the lateral resolution and 7.2 µm for the axial resolution. This indicates that the distribution of light intensity, above $1/e^2$ of the maximal intensity, occupies a volume that is close to the size of a single varicosity (Pulido et al., 2015).

Brain tissue will significantly scatter the 405-nm light used here for photolysis (Trigo et al., 2009a), making the actual point-spread function in the slice wider than the one measured in the preceding paragraph. To functionally test the spatial resolution, we performed a series of experiments in which the laser was sequentially

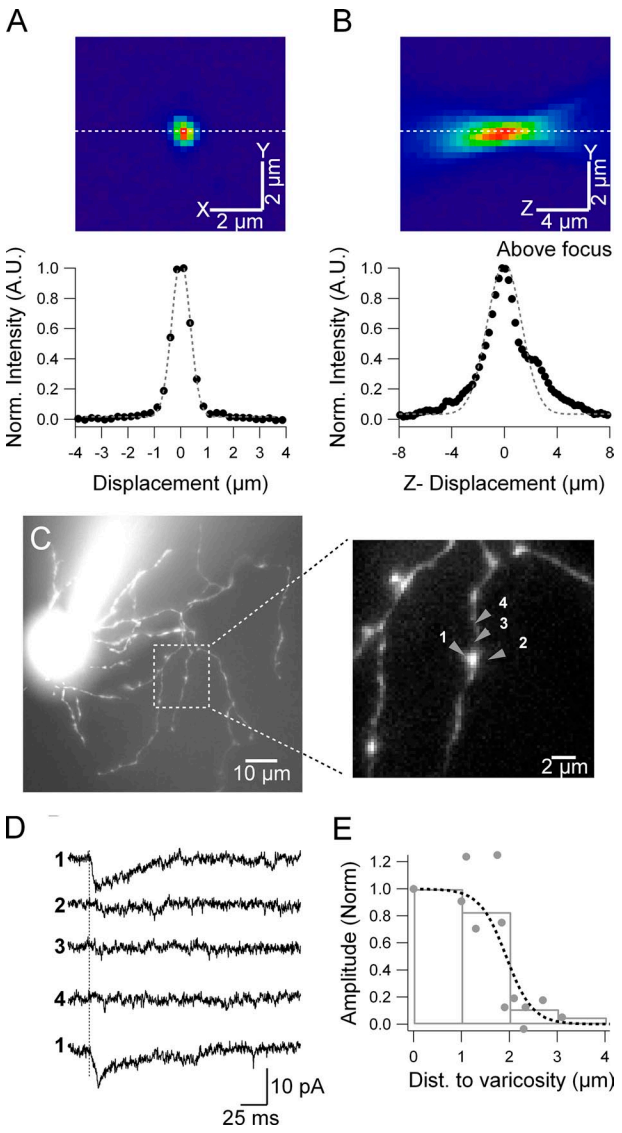

Figure 3. The spatial resolution of the Ca^{2+} photolysis approach permits evoking ASCs from single varicosities. Light intensity distribution of the laser spot. The laser beam was reflected back to the camera with a planar mirror placed at the level of the slice chamber and recorded with the EM-CCD camera. Stack of images made by changing the focus at 0.1-µm intervals. (A and B) The XY and YZ projections of the laser spot, respectively (bars, 2 µm). The bottom graphs show the intensity profile of the spot measured on the x axis (A) and on the z axis (B) at the level of the intensity peak ($1/e^2$ diameter for the x axis: 1.4 µm and for the z axis: 7.2 µm). (C) Stack of epifluorescence images of an Alexa Fluor–filled MLI (left) and detail of a section of the axon (right). The photolysis positions are marked with arrowheads and numbers. (D) Individual traces recorded while sequentially stimulating the positions indicated in C. Vertical dotted line indicates the timing of the laser pulse. (E) Amplitudes (normalized in 1-µm bins to the response evoked on the varicosity center) as a function of the distance between the stimulated position and the center of the varicosity (for this analysis, only the positions located on the axon were considered). Gray circles correspond to the amplitudes from individual sweeps. Continuous line shows the fit with a Gaussian function, with a half-width of 2.18 ± 0.28 µm (mean ± SEM; $n = 6$ sites).

pointed to the center of a varicosity and to nearby positions. An example is shown in Fig. 3 (C and D). Focusing the laser on the center of the varicosity produced ASCs, whereas illumination of nearby positions, either within or outside the axon, failed to produce any detectable response (numbered arrows in Fig. 3 C; inset indicates the positions of the laser spot during each sweep; the corresponding traces are shown in D). Increasing the distance to the center of the varicosity produced the loss of the response without any gradual decrease, consistent with the evoked ASCs originating from single release sites (Fig. 3 E). To estimate the resolution of the method to evoke ASCs, we measured the half-width of the Gaussian fit performed on the amplitude versus distance plot, giving 2.18 ± 0.28 µm (n = 7 sites, 5 cells; Fig. 3 E). This, together with immunostaining results presented below, showing a mean distance between varicosities of 6.1 ± 5.8 µm (Fig. 5 F), indicates that the laser-photolysis approach presented here allows us to evoke synaptic GABA release from individual varicosities. This puts us in the position to study the impact of single site–mediated axonal synaptic events on the activity of MLIs.

Laser-evoked ASCs are heterogeneous across release sites

Fig. 4 (A and B) shows a cell in which we performed caged-Ca^{2+} photolysis in five different release sites; the amplitudes and kinetics of the events arising from the stimulation of the different release sites were variable (amplitudes: 15–35 pA, coefficient of variation [CV] = 0.32). The amplitude distribution of ASCs recorded across all experiments is shown in the gray histogram of Fig. 4 C; it represents a wide range of values and displays a marked skew toward large values. Each color histogram and corresponding Gaussian fit are examples of the amplitude distributions of the events evoked in single varicosities; they show that, although inter-site variability is high, intra-site variability is low, similarly to what was estimated for the inter-site variability of postsynaptic responses in individual synapses (Auger and Marty, 1997; Nusser et al., 1997). The amplitudes in individual varicosities could be described by a Gaussian distribution, and the average coefficient of variation estimated from individual sites was significantly smaller than the coefficient of variation calculated from the amplitudes corresponding to all the stimulated varicosities (CV_{ind}: 0.16 ± 0.02; n = 41 varicosities; CV_{all} = 0.55; n = 64

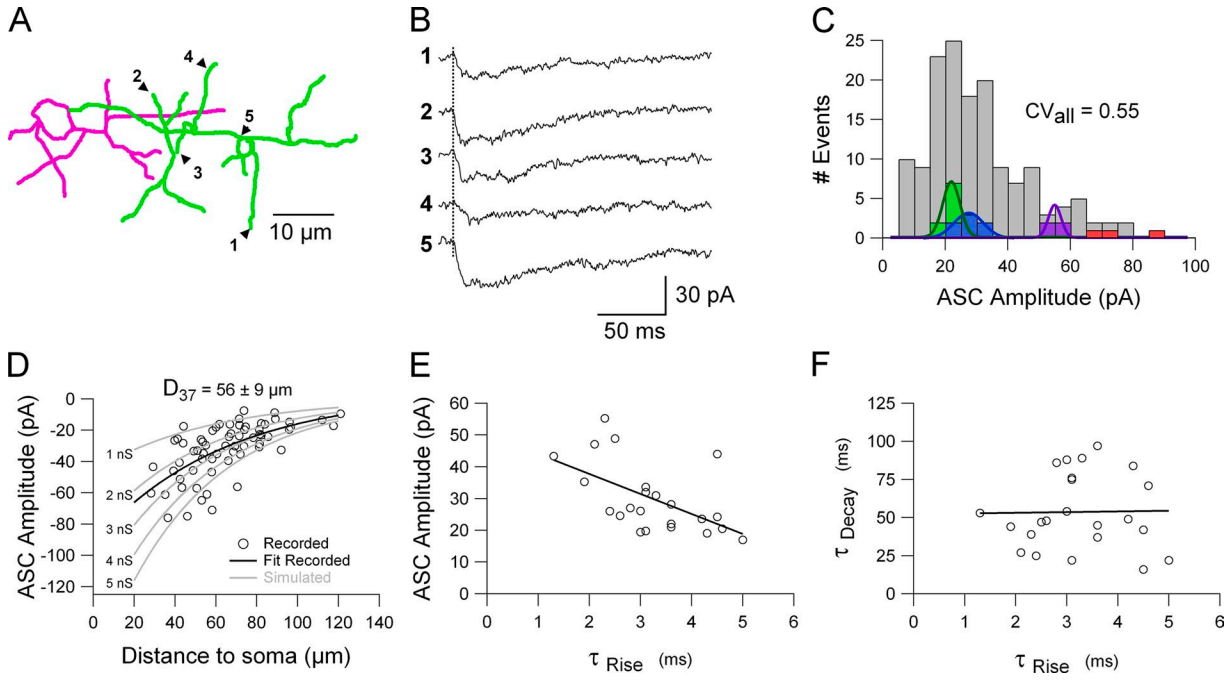

Figure 4. Axonal synaptic events are filtered by the axon. (A) Schematic reconstruction of an MLI that was successfully stimulated in several axonal varicosities (arrowheads; somatodendritic domain is in magenta, and axon is in green). (B) Representative traces of individual ASCs evoked in the positions indicated in A. The vertical dotted line indicates timing of the laser pulse. (C) Amplitude distribution of all the recorded ASCs (gray; n = 64 sites from 33 cells) and from four selected individual sites to illustrate the degree of intra-site variability (colored histograms and associated Gaussian fits, n = 3–12 events/site). (D) Plot of ASC amplitude as a function of the distance between the soma and the release site. Each circle represents an individual experiment; continuous black line is the exponential fit. The distance at which the amplitudes are reduced to 37% of their extrapolated maximal amplitude (D_{37}) is 56 ± 9 µm (n = 64 sites). Gray lines are the fits of simulated datasets using different autoR synaptic conductance values. The simulation performed with a 3-nS autoR synaptic conductance best fitted experimental data (Chi^2 values corresponding to the simulations with 1-, 2-, 3-, 4-, and 5-nS autoR conductance: 467.7, 174.3, 166.7, 259.6, and 395.0, respectively). (E) Plot of ASC amplitude as a function of τ_{rise}. Continuous line is the linear fit ($P < 0.01$; Pearson's coefficient: −0.56; n = 23 sites). (F) Plot of ASC τ_{decay} as a function of τ_{rise}. Continuous line is the linear fit ($P > 0.05$; Pearson's coefficient: 0.02; n = 23 sites).

sites; $P < 0.0001$). As an example, in the cell shown in Fig. 2, the amplitude CV of the seven laser-evoked currents was as low as 0.11. Collectively, these results suggest the existence of heterogeneities among the different release sites within a cell and between cells.

Single-site ASCs are generated in the axon and recorded in the soma. On their way to the somatic compartment, the propagating currents are affected in amplitude and time course by the axonal membrane–passive properties (e.g., axonal diameter, membrane resistance, and axial resistance; Rall, 1967). To directly assess the degree of filtering of ASCs by the axon and obtain a quantitative estimation of it, we evoked GABA release using laser photolysis of caged Ca^{2+} in individual varicosities at varying distances from the soma. ASC amplitudes followed an exponential relationship with the distance between the release site and the soma, as expected for a passive filter (black line in Fig. 4 D). The distance at which the amplitudes decreased to 37% of the back-extrapolated somatic amplitude (D_{37}) was 56 ± 9 µm (n = 64 sites; Fig. 4 D). Furthermore, consistent with Rall's passive filtering theory, we found a negative correlation between ASC amplitude and τ_{rise} ($P < 0.01$; Pearson's coefficient: −0.56; n = 23 sites; Fig. 4 E), and no correlation between τ_{decay} and τ_{rise} ($P > 0.05$; Pearson's coefficient: 0.02; n = 23 sites; Fig. 4 F).

To estimate the average autoR conductance corresponding to a single release site, we simulated autoR-mediated synaptic inputs in MLIs using the NEURON platform (Hines and Carnevale, 1997). Model MLIs consisted of two parts: the somatodendritic compartment, modeled as a small cylinder with passive conductances (diameter, 10 µm; length, 10 µm), and the axon, modeled as a thin and long cylinder with both passive and active conductances (diameter, 0.5 µm; length, 200 µm). The parameters for the simulations were taken from previously validated models (see Materials and methods). Previous work has shown that in MLIs, both somatodendritic and axonal $GABA_A$Rs contain the low affinity, fast kinetics–conferring α1 subunit (Stell et al., 2007; Trigo et al., 2007); therefore, we modeled the decay kinetics of axonal $GABA_A$Rs based on the kinetics of somatodendritic receptors. Simulated ASCs faithfully reproduced the filtering shown in Fig. 4 D. To estimate the mean autoR conductance, we repeated iteratively the simulation using different autoR conductance values (continuous gray lines in Fig. 4 D) and compared the goodness of fit to the experimental data (open circles in Fig. 4 D). The conductance value that best described the experimental data was 3 nS, although the observed amplitudes fell within a wide range of conductances (1–5 nS), reflecting a high degree of variability between sites. These results indicate that ASC conductance values are surprisingly similar to the values that have been estimated before for dendritic GABAergic responses, suggesting that pre- and postsynaptic varicosities have a similar number of $GABA_A$Rs (see Discussion).

GABA release sites are heterogeneously distributed along the axon

Axonal anatomy (length, number of branching points, etc.) as well as the number and distribution of GABA release sites are critical parameters that define the impact of $GABA_A$ autoR activation on the activity of MLIs. Previous studies estimated the density of GABA release sites in MLIs either by quantifying axonal varicosities in neurobiotin-filled cells (Pouzat and Hestrin, 1997) or by recording Ca^{2+} "hot spots" with two-photon microscopy (Forti et al., 2000). However, information about their spatial distribution in the axon is still lacking.

To quantify GABA release sites in individual cells, we filled MLIs with Alexa Fluor 488 (Fig. 5 A) and immunolabeled presynaptic GABAergic specializations using antibodies against VGAT (Fig. 5 B). We used Vaa3D software (Peng et al., 2010) to make 3-D reconstructions of MLIs based on Alexa Fluor 488 staining and measured VGAT-labeling intensity within the reconstructed cells. As shown in Figs. 1–3, the morphology of young MLI axons is relatively simple: it comprises a main branch and secondary collaterals that, in general, emerge perpendicularly. We performed immunofluorescence labeling and morphological measurements in seven MLIs. The mean main branch length of the reconstructed axons was 211.7 ± 54.9 µm and, on average, each axon had 16 ± 5 collaterals. In some cases, tertiary collaterals were found, but these were not taken into consideration because of their small number and size. The intensity profile of VGAT staining along the axon of reconstructed MLIs showed a dense labeling in the somatic region, followed by segments where basal fluorescence was interrupted by peaks of high intensity that correspond to GABA release sites (Fig. 5 D), usually located in axonal varicosities (observed as enlargements of the axonal diameter and as peaks in the Alexa Fluor intensity; Fig. 5 D, right). VGAT spots inside the reconstructed MLIs were clearly identified by colocalization with Alexa Fluor, as shown in Fig. 5 C (note colocalization both in XY and XZ projections). Fig. 5 E shows the number of release sites along the whole axonal branch. Release sites were found all along the reconstructed axons, although their distribution was not homogeneous. The portion of the axon with the highest concentration of release sites was the second quarter (mean number of release sites, 12.4 ± 5.2; n = 7 MLIs; Fig. 5 E). The average total number of GABA release sites was 68 ± 28 sites/axon, and the mean distance between sites was 6.1 ± 5.8 µm (Fig. 5 F). The portion of the axon with the highest number of branches was also the second quarter (mean number of branches, 8.2 ± 3.7; n = 7 MLIs; Fig. 5 G); the length of the branches was short (mean, 24.1 ± 18.8 µm; median, 19.4 µm; Fig. 5 H). Given

that the density of sites was independent of branch location (not depicted), the concentration of VGAT spots in the second quarter can be explained by the higher number of collateral branches in this region of the axon. These results constitute the first anatomical description of the distribution of GABA release sites in juvenile MLI axons. Collectively, they show that in young MLIs, the axonal morphology is simple, comprising a single, main axonal branch with almost exclusively second-order collaterals.

So far, we have estimated some physiological and morphological properties of young MLI axons and their GABAergic release sites. The estimated autoR synaptic conductance, the degree of filtering, and the distribution of release sites all suggest that, in physiological conditions, the voltage signals generated in single axonal varicosities can backpropagate and sum with somatodendritic synaptic inputs. We explore this possibility in detail below.

Impact of ASCs on membrane potential

In young MLIs, E_{GABA} is more depolarized than in other cerebellar cell types and is highly variable as a result of heterogeneity in $[Cl^-]_i$ (estimated to be 15 mM on average; Chavas and Marty, 2003). Here, we examine the changes in the neuronal membrane potential produced by the activation of $GABA_A$ autoRs in physiological conditions. For this purpose, we recorded the cells in current clamp with a physiological intracellular solution containing 15 mM Cl^- and evoked local GABA release using caged-Ca^{2+} photolysis. As mentioned before, in MLIs subthreshold somatodendritic depolarizations are transmitted to presynaptic terminals and induce an increase in the frequency of spontaneous axonal events or

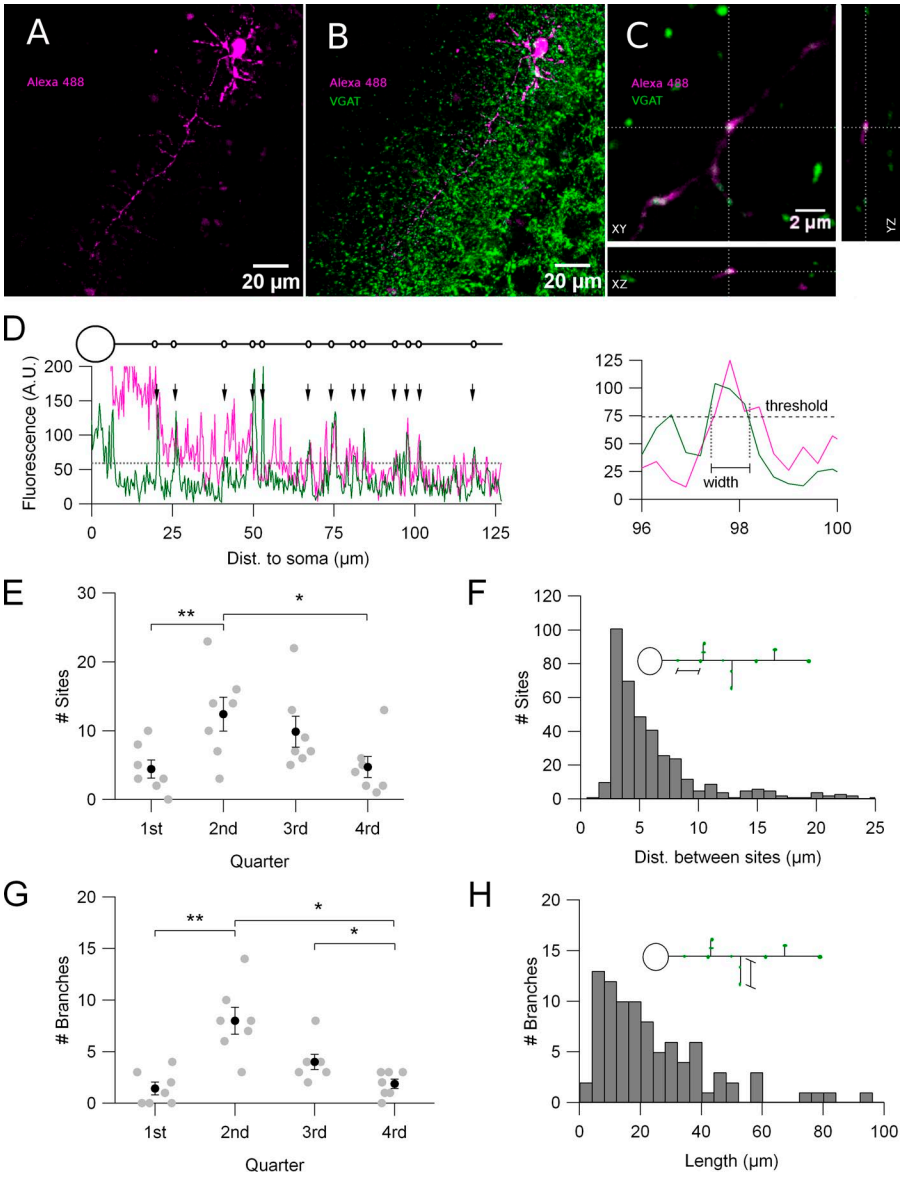

Figure 5. Quantification of the number and distribution of GABA release sites in MLI axons. Immunolabeling of VGAT in Alexa Fluor 488–loaded MLIs was performed to identify axonal release sites. (A) Confocal image stack Z projection of an Alexa Fluor 488–filled MLI. (B) Superimposition of Alexa Fluor (magenta) and VGAT immunolabeling (green). (C) Detail of the colocalization of VGAT and Alexa Fluor 488 labeling in a varicosity. XY, YZ, and XZ projections (middle, right, and bottom panels, respectively). (D) Intensity profiles of VGAT (green line) and Alexa Fluor 488 (magenta line) along the main branch of an MLI axon. The cartoon on top represents the MLI's soma and axonal main branch; circles indicate detected GABA varicosities. The soma produced an intense labeling while the rest of the trace showed near baseline intensity interrupted by clearly defined peaks of VGAT and Alexa Fluor intensity, corresponding to varicosities. (Inset) Criteria used for detecting release sites. Threshold = baseline + 2 SD of the VGAT intensity profile (green trace in D); width, >500 nm. GABA release sites are heterogeneously distributed along the axon. (E) Number of release sites per axonal quarter. (F) Histogram of distances between release sites (mean ± SD: 6.1 ± 5.8 µm; median: 4.4 µm; n = 390 pairs of sites). Branching points are also heterogeneously distributed along the axon. (G) Number of branches per axonal quarter. (H) Histogram of collateral's length (mean ± SD: 24.1 ± 18.8 µm; median: 19.4 µm; n = 89 collaterals). In E and G, the gray dots represent individual cells, and the black dots show mean ± SD; n = 7 reconstructed MLIs (*, $P < 0.05$; **, $P < 0.01$).

preminis (Trigo et al., 2010), all in an AP-independent manner. To study the impact of evoked, single-site responses and avoid any possible contribution of spontaneous events, membrane potential was kept near −70 mV by injection of negative current (−30 ± 4 pA; $n = 12$ cells). In these conditions, local caged-Ca^{2+} photolysis in the axon produced subthreshold depolarizing responses (Fig. 6 A; black traces are individual sweeps, and the gray trace is the average); we called the laser-evoked responses "autoR-mediated synaptic potentials" (ASPs), in analogy to the ASCs. ASP amplitudes were relatively big, and their timing clearly indicated the pairing with the laser pulse. The depolarizations shown in Fig. 6 A had an average amplitude of 5.0 mV and a decay time constant of 47 ms. Averaged traces revealed clear depolarizing responses with a mean amplitude among all the sites of 3.4 ± 0.4 mV (ranging from 1.2 to 6.4 mV), mean τ_{rise} of 9.2 ± 1.0 ms, and mean τ_{decay} of 92 ± 16 ms (21 sites; 17 cells; holding potential was between −67 and −76 mV). As expected for filtered signals, the ASP amplitude decreased as a function of the distance between the stimulated release site and the soma. Representative traces of ASPs evoked at 36, 45, 54, and 87 µm from the soma are shown in Fig. 6 B. A fit of the amplitudes plotted as a function of the distance between the release site and the soma with an exponential function gave a D_{37} value of 91 ± 66 µm ($n = 21$ sites; Fig. 6 C). Extrapolation of the ASP amplitude versus distance plot predicts

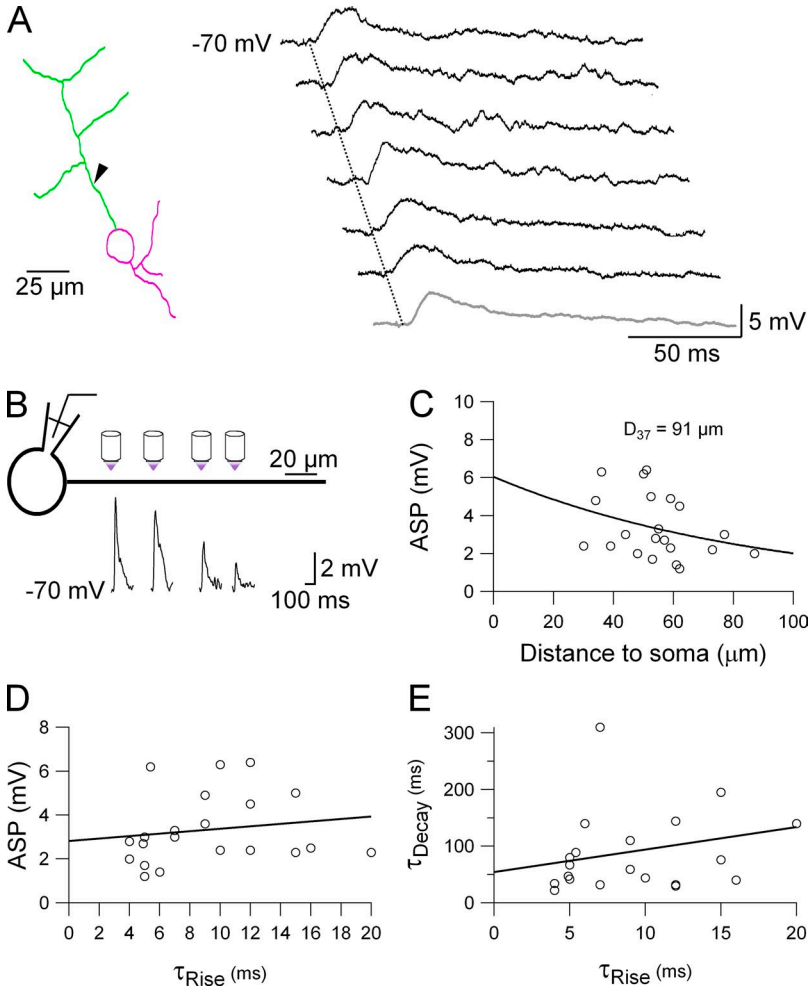

Figure 6. Subthreshold ASPs from single release sites backpropagate to the soma. (A) Representative current-clamp recordings of six consecutive ASPs (black) and their average (gray) evoked by local Ca^{2+} photolysis in an individual varicosity; the cell was recorded at physiological $[Cl^-]_i$ (15 mM) and kept at a −70-mV holding potential; the dotted gray line indicates timing of the laser pulse. The reconstruction on the left shows the location of the photolysis spot (arrowhead). (B) Average traces of ASPs evoked in four different release sites from different cells located at 36, 45, 54, and 87 µm from the soma (amplitudes were 6.3, 4.9, 2.8, and 2 mV, respectively; $n = 2$–10 events per site). (C) Plot of ASP amplitude as a function of the distance between the soma and the release site. Individual points correspond to average amplitudes made from 2 to 26 individual sweeps from single release sites. Continuous line is the exponential fit ($D_{37} = 91 \pm 66$ µm; $n = 21$ sites). (D) Plot of ASP amplitude as a function of τ_{Rise} (continuous line is the linear fit; $P > 0.05$; Pearson's coefficient = 0.61; $n = 21$ sites). (E) Plot of τ_{Decay} as a function of τ_{Rise} (continuous line is the linear fit; $P > 0.05$; Pearson's coefficient = −0.24; $n = 21$ sites).

nonfiltered (in situ) local amplitudes of ~6 mV. Interestingly, contrary to predictions for a passive filter (Rall, 1967) and to the results obtained in voltage clamp (Fig. 4 E), there was no significant negative correlation between the ASP amplitude and τ_{rise} (Fig. 6 D), and no correlation between τ_{decay} and τ_{rise} (Fig. 6 E). These results show for the first time that, in physiological conditions, axonal depolarizations from individual release sites can backpropagate and produce substantial somatic depolarizations.

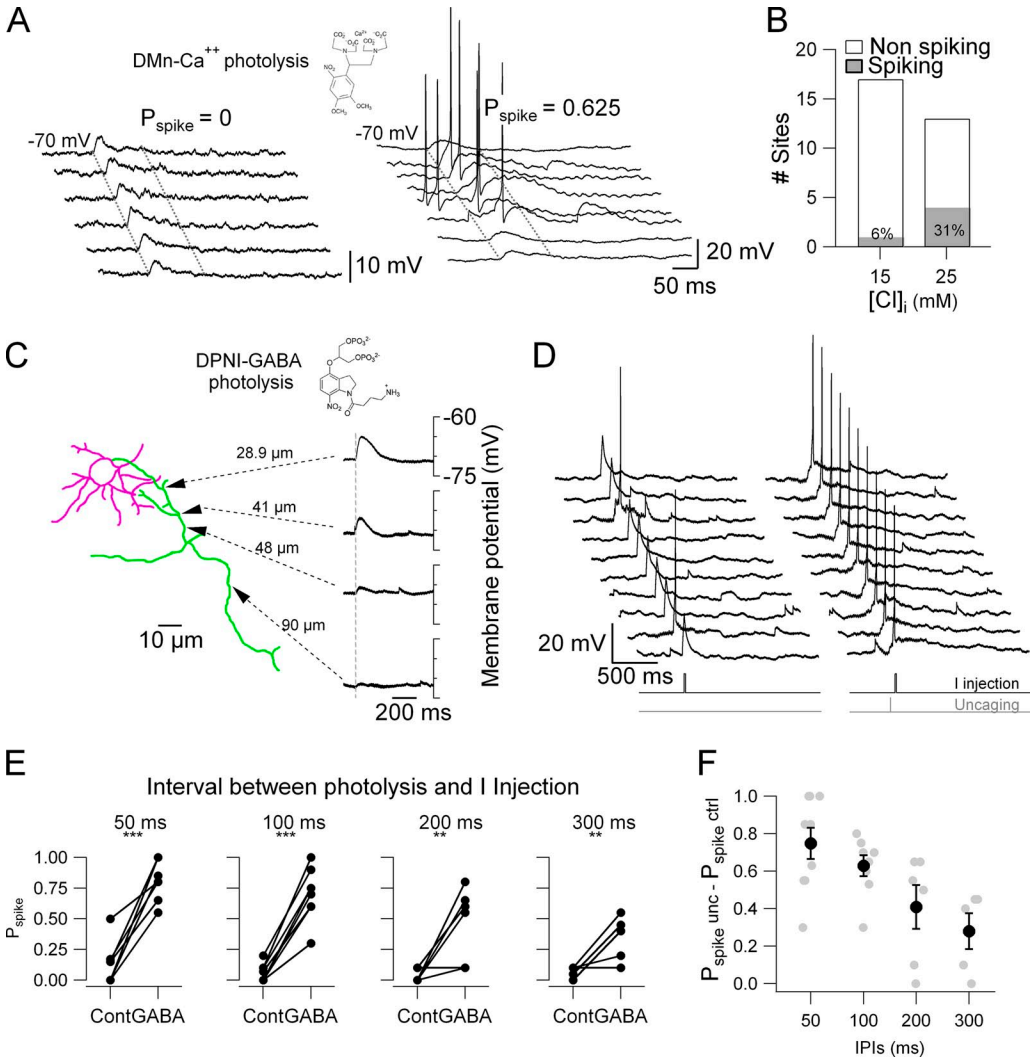

Figure 7. Axonal $GABA_A$Rs activation in single presynaptic varicosities has a marked effect on MLI excitability. (A; left) Representative traces of laser-evoked ASPs recorded in current-clamp mode with an intracellular solution containing $[Cl^-]_i$ = 15 mM. In this cell, photolysis of caged Ca^{2+} produced subthreshold depolarizing responses (same cell as in Fig. 6 A), with a P_{spike} of 0. (Right) Laser-evoked ASPs recorded in the same condition as shown in the left panel. In this cell, the ASPs induced AP firing with a probability P_{spike} of 0.625. (B) Summary plot of the fraction of release sites that produced active responses with 15 and 25 mM $[Cl^-]_i$. The percentage of release sites that produced active responses in each experimental condition is shown in the bars (n = 17 sites with $[Cl^-]_i$ = 15 mM and 13 sites with $[Cl^-]_i$ = 25 mM). (C) Example of an MLI where GABA was photolyzed from DPNI-GABA (1 ms, 2-mW pulses) in four different axonal locations. Traces are averages from four to five sweeps, with amplitudes 5.5, 4.0, 1.7, and 0.6 mV; Vm values −70.8, −70.7, −67, and −72 mV (average values during 100 ms before the laser pulse); and distances to the soma 28.9, 41, 48, and 90 µm, respectively. Gray dotted line indicates timing of the laser pulse. (D) Somatic whole-cell recordings in current-clamp mode of the responses to current injection without (left) and with (right) prepulses of caged-GABA photolysis in the axon (50-ms interval between photolysis pulse and current injection). It can be observed that P_{spike} increases dramatically with the GABA prepulse. (E) P_{spike} in control (Ctrl) and with caged-GABA prepulses (GABA) for different time intervals between the laser pulse and the current injection: 50, 100, 200, and 300 ms; **, P < 0.01; ***, P < 0.001. (F) The increase of P_{spike} produced by the photolysis of caged GABA was plotted as a function of the interval between the laser and the current-injection pulses. The excitability increase has a very similar time course when compared with the decay of the GABA-induced depolarizations. Gray circles are the values from individual cells; black symbols and error bars represent mean ± SEM for each time interval. The cells were held near −70 mV.

Activation of autoRs increases MLI excitability

In the previous section, we showed that local voltage changes that arise locally in the axon by the activation of $GABA_A$ autoRs in single varicosities backpropagate to the soma. Our immunolabeling results show that a significant number of varicosities are localized close to the soma and may therefore influence the membrane potential (Vm) in the axon initial segment (AIS) substantially. This, together with the fact that MLIs have a high input resistance (Midtgaard, 1992; Llano and Gerschenfeld, 1993), made us hypothesize that single axonal synaptic events, although filtered, may strongly influence neuronal firing (as was shown previously for somatodendritic glutamatergic events; Carter and Regehr, 2002). A first indication that this is indeed the case appeared when performing the experiments in Fig. 6. As mentioned above, although most of the stimulated release sites produced subthreshold responses (16 out of 17 sites; Fig. 7 A, left), in one exceptional cell, DM-nitrophen photolysis lead to direct AP firing (Fig. 7 A, right; we quantified this excitability change as the probability of observing an AP during 100 ms after the laser stimulation: P_{spike}). To test the impact of $[Cl^-]_i$ heterogeneity among cells, we performed another set of experiments where we increased $[Cl^-]_i$ to 25 mM ($E_{GABA} = -45$ mV, within the range of observed values; Chavas and Marty, 2003). In these conditions, 31% (4 out of 13) of the stimulated sites had $P_{spike} > 0$, with values ranging from 0.2 to 0.308 (mean $P_{spike} = 0.265$; $n = 13$ sites, 13 cells; 3–12 laser stimulations per site; Fig. 7 B).

MLIs receive GABAergic synaptic inputs from other interneurons and glutamatergic synaptic inputs from granule cells. To study the interaction between somatodendritic synaptic inputs and axonal, GABAergic synaptic inputs on MLI excitability, we performed a series of experiments where we applied depolarizing current pulses with and without previous local GABA photorelease pulses. Caged-GABA was preferred to caged-Ca^{2+} photolysis because it allowed us to perform numerous repetitions with no evidence of photodamage (see Materials and methods). Photolysis of caged GABA from the caged compound DPNI-GABA (1 ms; 2-mW pulses) on axonal varicosities evoked responses with characteristics similar to the DM-nitrophen-Ca^{2+}–evoked responses. As shown in Fig. 7 C, the amplitudes of the DPNI-GABA–evoked responses showed the same distance dependence to the soma. The amplitudes were slightly but significantly larger than those evoked by intracellular caged-Ca^{2+} photolysis (GABA, 4.6 ± 0.5 mV; Ca^{2+}, 3.3 ± 0.5 mV; $P < 0.05$; $n = 9$–24 cells; $[Cl^-]_i = 15$ mM); this difference can be explained by the slightly larger volume over which GABA spreads when it is photoreleased (Trigo et al., 2009b) compared with synaptic release, and also to the larger photolysis volume (DM-nitrophen is intracellular, whereas DPNI-GABA is extracellular). To mimic somatodendritic synaptic inputs, we used current injection pulses that were adjusted to bring Vm close to spike threshold (injected current, 13–55 pA; duration, 20 ms), setting a low P_{spike} probability. P_{spike} was calculated from 10 sweeps in each condition: control (without GABA photolysis) and with GABA photolysis at four different time intervals between the laser pulse and the current injection (50, 100, 200, and 300 ms). Fig. 7 D shows an example: the left traces represent the depolarization induced by the current injection alone, and the right traces represent the depolarizations induced when the current injection pulse was preceded (50 ms) by a GABA photolysis pulse in the axon. Paired analysis of P_{spike} in control and after GABA uncaging revealed that local GABA prepulses applied in axonal varicosities increased excitability at all time intervals (Fig. 7, E and F). The time course of the facilitating effect on cellular excitability is very similar to the time course of the axonal membrane potential changes, indicating that the increase in the excitability is directly dependent on depolarization. Collectively, these results demonstrate that although the activation of presynaptic varicosities produces small somatic voltage changes, the end effect on cell excitability can be strong and turn subthreshold signals originating in the somatodendritic compartment into suprathreshold events.

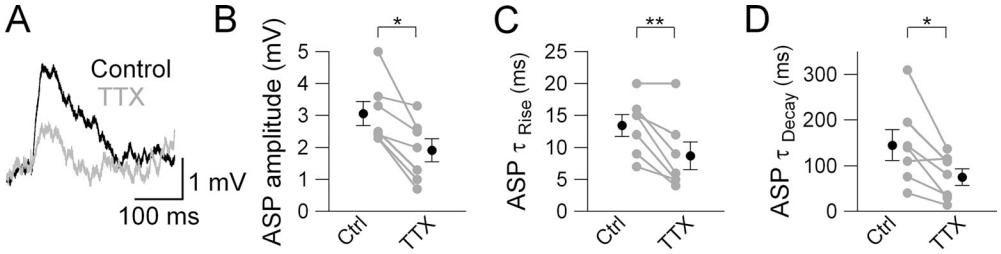

Figure 8. AutoR-mediated responses are amplified by activation of Na_v channels. (A) Representative traces of average laser-evoked ASPs in control (black) and in TTX (gray; 400 nM). Summary plot of TTX effect on (B) ASP amplitude (control: 3.1 ± 1 mV; TTX: 1.9 ± 1 mV; paired *t* test, **, $P < 0.01$; $n = 7$ sites), (C) τ_{Rise} (control: 13 ± 4 ms; TTX: 9 ± 4 ms; paired *t* test, **, $P < 0.01$; $n = 7$ sites), and (D) τ_{Decay} (control: 145 ± 88 ms; TTX: 75 ± 48 ms; paired *t* test, *, $P < 0.05$; $n = 7$ sites). Black dots represent mean ± SEM.

AutoR-mediated responses are amplified by Na_v conductances

Some of the results obtained so far suggest that the autoR-mediated depolarizations are not exclusively passive, but involve an active mechanism: first, the finding that ASPs are capable of triggering APs; second, the lack of negative correlation between τ_{rise} and ASP amplitude (Fig. 6 D); third, the fact that τ_{decay} of ASPs is systematically longer than 32 ms, the membrane time constant that has been calculated for MLIs (Mejia-Gervacio et al., 2007); and last, the longer D_{37} in current clamp (Fig. 6 C) compared with the one in voltage clamp (Fig. 3 D). To test the hypothesis that autoR-mediated responses also involve the activation of an active mechanism, most likely Na_v conductances, we performed calcium photolysis experiments, both in control and in the presence of TTX. As can be seen in Fig. 8, adding TTX to the bath solution significantly reduced the amplitude of laser-evoked ASPs in 15 mM $[Cl^-]_i$ (Fig. 8, A and B). Furthermore, TTX accelerated the kinetics of the responses, reducing τ_{rise} (Fig. 8 C) and τ_{decay} (Fig. 8 D). Collectively, these results show that $GABA_A$ autoR-mediated, single-site depolarizations are amplified by the activation of a Na_v conductance; this amplification mechanism is a unique feature of the axonal compartment of interneurons.

DISCUSSION

Our results show that in cerebellar MLIs, activation of single axonal varicosities by release of GABA from a single synapse can alter interneuron excitability. This effect depends on a combination of factors: high autoR conductance value, proximity of axonal varicosities to the somatic compartment, simple axonal geometry, high membrane resistance, and interaction of the autoR conductance with an active sodium conductance. We conclude that individual ASCs carry a strong feedback signal that can have a profound impact on MLI activity.

AutoR-mediated synaptic responses

GABA release from individual varicosities consistently activated a large presynaptic conductance mediated by $GABA_A$Rs. Extrapolation of the ASC amplitude versus distance plot at high $[Cl^-]_i$ (Fig. 4 D) predicts a nonfiltered (in situ) amplitude of ~100 pA. In equivalent experimental conditions, Llano and Gerschenfeld (1993) reported somatodendritic GABAergic postsynaptic currents ranging between 61 and 226 pA. Assuming a single-channel conductance of 30 pS for $GABA_A$Rs (Bormann et al., 1987), and considering the range of values found for the autoR conductances (1–5 nS), we estimate that each presynaptic varicosity is endowed with 33–167 channels. This is similar to the estimates of Auger and Marty (1997) and Nusser et al. (1997) for the number of $GABA_A$Rs in postsynaptic densities in the same synapse (9–102 and 6–380 channels/synapse, respectively) and the estimation done by electron microscopy with immunogold labeling of the α1 subunit of $GABA_A$Rs in the MLI to Purkinje cell synapse (Trigo et al., 2010). It needs to be noted, however, that the autoR conductance estimates come from measurements of the amplitudes of ASCs that are mainly multi-vesicular (compared with dendritic miniature events, mainly uni-vesicular). Therefore, the estimate of the number of $GABA_A$Rs in presynaptic varicosities should be considered an upper value. In summary, our results show that, in MLIs, presynaptic varicosities and postsynaptic densities have a similar number of $GABA_A$Rs. This is a striking result; indeed, the presynaptic signal delivered by the activation of $GABA_A$ autoRs in a single varicosity is almost as large as the postsynaptic signal.

It has been shown previously that there is a positive correlation between the size of the active zone and that of the postsynaptic density (Schikorski and Stevens, 1997; Harris and Stevens, 1988); likewise, the size of the postsynaptic density determines the quantal size: a larger postsynaptic area allows a higher number of receptors (Auger and Marty, 1997; Nusser et al., 1997). Moreover, our recent evidence suggests that the size of the active zone is positively correlated with the RRP in presynaptic specializations (Trigo et al., 2012; Pulido et al., 2015). The variability observed on the amplitude of ASCs is probably caused by differences in the overall morphology of the synapses: bigger synapses have a larger active zone, a larger RRP, and a higher number of receptors.

Axonal filtering: Range of action of axonal single-site responses

Axonal filtering defines the distance up to which signals originating in a given release site propagate, i.e., their action range. In voltage-clamp mode and in high $[Cl^-]_i$, ASCs evoked at variable distances from the soma decayed to 37% of their back-extrapolated amplitude in 56 µm; ASPs recorded in current-clamp mode and physiological $[Cl^-]_i$ did so in 91 µm. The difference between the D_{37} values estimated in voltage and current clamp suggests that the amplification mediated by the Na_v conductance (see below) is an important determinant of the transmission of subthreshold voltage signals. Even though in current clamp the voltage changes are presumably shunted by the activation of the autoRs and the subsequent activation of the Na_v conductance, the amplification produced by the latter seems to prevail and prolongs D_{37}. At the same time, the axonal space constant (λ) estimated by computational simulation was 434 µm (not depicted), consistent with previous estimates (Pouzat and Marty, 1999; Mejia-Gervacio et al., 2007). The difference between these two values may be caused by: (a) the shunting effect produced by the activation of the autoRs and the Na_v channels and (b) the low-pass filtering effect of the axonal membrane, which affects fast synaptic signals, whereas the spatial constant

is defined for the steady state. In summary, considering that the average length of MLI axons at this age is around 200 µm, our results indicate that in spite of passive filtering, autoR-mediated synaptic signals propagate over a substantial part of the axonal compartment.

Interaction between autoR responses and Na_v channels

AutoR responses were partially blocked by the addition of TTX to the bath, indicating that the responses in control condition are enhanced by voltage-dependent Na^+ channels. This is consistent with the presence of a prominent, persistent Na_v conductance in these cells (Mann-Metzer and Yarom, 2002). This conductance type is characterized by its hyperpolarized activation threshold, which makes MLI axons particularly reactive to subthreshold depolarizations. Huang and Trussell (2008) reported an activation threshold of −85 mV and a V_{half} of −55 mV for the persistent Na_v current in the Calyx of Held; a similar result was found by Carter et al. (2012). If we consider that E_{GABA} = −58 mV (estimated with the $[Cl^-]_i$ used), this value falls within the voltage range where $GABA_A$Rs can be depolarizing. Thus, even if the driving force for axonal $GABA_A$Rs is relatively small, the synergy with persistent Na_v channels can enhance depolarizations. In that sense, Carter et al. (2012) found that depolarizations as small as 1 mV in dendrites are enough to engage the Na^+ current. In brainstem, hippocampal and cortical neuron E_{GABA} is more depolarized in the axon than in the soma or dendrites (Price and Trussell, 2006; Khirug et al., 2008), suggesting that in MLIs, the reversal potential for autoR-mediated responses could be even more depolarized than the above value. The activation of the Na_v conductance and the subsequent amplification effect contrast with the purely passive behavior of MLI dendrites (Abrahamsson et al., 2012) and highlight the importance of studying the integrative properties of axons.

Possible physiological role

The activation of axonal autoRs can have global and local effects. Concerning global effects, it was shown before that the simultaneous activation of the $GABA_A$ autoRs from many release sites by the AP-evoked release of GABA increases firing probability (Mejia-Gervacio and Marty, 2006). We show here that in conditions of physiological intracellular chloride (15 mM), the release of GABA from a single varicosity produces local voltage changes that are transmitted antidromically and alter the somatic Vm. Together with subthreshold somatodendritic depolarizations, ASPs lead to a drastic increase in P_{spike} that very often leads to AP firing. These results are not surprising considering that MLIs are small, electrically compact cells with high input resistances (>1 GΩ; Llano and Gerschenfeld, 1993), where single synaptic inputs can shape cell firing (Carter and Regehr, 2002).

VGAT immunolabeling revealed a concentration of GABA release sites in the proximal part of the axon, close to the AIS; more specifically, ∼30% of the synapses are separated from the soma by a distance shorter than that representing the 1/e decay of autoR-mediated signals (91 µm) and therefore can modify the membrane potential in the AIS (the spike initiation site). Thus, even if the single-site activation of axonal $GABA_A$Rs does not induce direct cell firing, ASPs can interact with somatodendritic synaptic events and modulate firing activity. This is supported by our experiments in Fig. 7. When extracellular GABA photolysis (to mimic the activation of axonal $GABA_A$Rs) is combined with somatic current injection pulses (to mimic glutamatergic somatodendritic synaptic inputs), the excitability of the cell changes dramatically. Because the potential change has a slow decay, this excitability change lingers for a rather long interval (up to 300 ms) between the current injection and the photolysis pulses. Collectively, these data indicate that the axon of MLIs operates as an integration compartment and support the notion that local signals arising primarily in the axon can be transmitted antidromically and influence neuronal excitability, as was proposed previously (Paradiso and Wu, 2009; Pugh and Jahr, 2013).

Because the source of GABA driving the activation of autoRs is the MLIs itself, ASCs constitute a feedback mechanism that may be used to control interneuron excitability. This mechanism shares the same signaling molecules as classical pre- to postsynaptic neurotransmission and thus provides the system with two distinctive features: high temporal precision, on the time scale of synaptic transmission, and target selectivity, caused by the constraints that the synapse imposes to diffusion of the neurotransmitter. The physiological effect of autoR activation (excitation, shunt, inhibition) depends on the relationship between E_{GABA} (estimated for somatodendritic events as −58 mV; Chavas and Marty, 2003; see below) and Vm at the time of vesicle fusion, which changes continuously according to the cell's activity. At hyperpolarized potentials, as those used in this study, very few fusion events will occur and very few varicosities will be activated (Trigo et al., 2010). If one such varicosities is activated, it will produce a depolarization, increasing the excitability of the cell and facilitating transmitter release. At depolarized potentials, many varicosities will be activated simultaneously, hyperpolarizing and/or shunting the axon. In this scenario, autoRs may be acting as a buffer for the spiking activity in the axon.

Besides their effects on cellular excitability, autoRs can alter locally the release properties of the releasing varicosity as well as of its neighbors. If we consider the estimated in situ membrane potential change of 6 mV, Vm will change by around 2 mV at the 1/e action range (91 µm) of a single release site. The average inter-site distance is 6 µm (Fig. 5 F), so that within the estimated

91-µm action range, the activation of a single release site will lead to substantial changes in the membrane potential of 14.5 neighboring synapses. These "local" changes in Vm may produce substantial modifications in transmitter release, in a fashion similar to the analogue-signaling mechanism described in Bouhours et al. (2011), Christie et al. (2011), and Glitsch and Marty (1999), and other preparations (Shu et al., 2006; Alle and Geiger, 2007; Debanne et al., 2013).

E_{GABA} in the axon of MLIs

The excitatory effect of single-site, autoR-mediated events observed in this work relies on a relatively depolarized E_{Cl} in relation to the resting potential of the cell. In this work, we used $[Cl^-]_i$ = 15 mM, which is the mean intracellular chloride concentration estimated previously by Chavas and Marty (2003) for the somatodendritic compartment of MLIs, but the exact $[Cl^-]_i$ in the axon of MLIs is not known. Our previous work shows that axonal $GABA_AR$ activation increases GABA release, indicating that axonal E_{GABA} is depolarized (Trigo et al., 2007). Evidence from other neuronal types likewise indicates a high axonal $[Cl^-]_i$ and, in some cases, the existence of a $[Cl^-]_i$ gradient between somatodendritic and axonal compartments. Examples include terminals of neurohypothalamic cells (Zhang and Jackson, 1995), terminals of retinal cells (Billups and Attwell, 2002), calyceal terminals in the brainstem (Price and Trussell, 2006), the AIS of cortical neurons (Szabadics et al., 2006; Khirug et al., 2008), hippocampal mossy fiber boutons (Ruiz et al., 2010), primary afferent terminals in the spinal cord (Eccles et al., 1962), and cerebellar parallel fibers (Stell et al., 2007; Pugh and Jahr, 2011, 2013; Dellal et al., 2012). To our knowledge, a single article reported evidence supporting a hyperpolarizing effect of axonal $GABA_ARs$ (Glickfeld et al., 2009). Overall, it appears that high $[Cl^-]_i$ and depolarizing GABAergic responses are general features of the axonal compartment of central neurons.

Possible role of axonal AutoRs in network/cell maturation

AutoR responses are age dependent and disappear around postnatal day 15 (Pouzat and Marty, 1999; Mejia-Gervacio and Marty, 2006; Trigo et al., 2010), a period in which the molecular layer acquires its mature morphology and functionality. $GABA_ARs$ are involved in the consolidation of GABAergic networks (Ben-Ari, 2002; Wang and Kriegstein, 2009), which suggests that axonal $GABA_ARs$ may be involved in MLI maturation. Because their activation affects spiking activity, it could be interpreted as a handshaking mechanism that reports to the rest of the network the functionality of the newly formed synapses and the state of maturation of the cell.

The authors would like to thank Philippe Ascher, María del Pilar Gómez, Isabel Llano, Alain Marty, Enrico Nasi, David Ogden, and Brandon S. Stell for helpful discussion and critical reading of the manuscript.

This work was supported by a combined Centre National de la Recherche Scientifique/Paris Descartes Excellence Chair (to F.F. Trigo), Fondation pour la Recherche Médicale (contract no. SPF20130526621; J. Zorrilla de San Martin), and ERC "Single-Site" (to Alain Marty; AG nb. 294509).

The authors declare no competing financial interests.

Richard W. Aldrich served as editor.

Submitted: 2 September 2015
Accepted: 13 October 2015

REFERENCES

Abrahamsson, T., L. Cathala, K. Matsui, R. Shigemoto, and D.A. Digregorio. 2012. Thin dendrites of cerebellar interneurons confer sublinear synaptic integration and a gradient of short-term plasticity. *Neuron.* 73:1159–1172. http://dx.doi.org/10.1016/j.neuron.2012.01.027

Alle, H., and J.R.P. Geiger. 2007. GABAergic spill-over transmission onto hippocampal mossy fiber boutons. *J. Neurosci.* 27:942–950. http://dx.doi.org/10.1523/JNEUROSCI.4996-06.2007

Auger, C., and A. Marty. 1997. Heterogeneity of functional synaptic parameters among single release sites. *Neuron.* 19:139–150. http://dx.doi.org/10.1016/S0896-6273(00)80354-2

Ben-Ari, Y. 2002. Excitatory actions of gaba during development: the nature of the nurture. *Nat. Rev. Neurosci.* 3:728–739. http://dx.doi.org/10.1038/nrn920

Billups, D., and D. Attwell. 2002. Control of intracellular chloride concentration and GABA response polarity in rat retinal ON bipolar cells. *J. Physiol.* 545:183–198. http://dx.doi.org/10.1113/jphysiol.2002.024877

Bormann, J., O.P. Hamill, and B. Sakmann. 1987. Mechanism of anion permeation through channels gated by glycine and gamma-aminobutyric acid in mouse cultured spinal neurones. *J. Physiol.* 385:243–286. http://dx.doi.org/10.1113/jphysiol.1987.sp016493

Bouhours, B., F.F. Trigo, and A. Marty. 2011. Somatic depolarization enhances GABA release in cerebellar interneurons via a calcium/protein kinase C pathway. *J. Neurosci.* 31:5804–5815. http://dx.doi.org/10.1523/JNEUROSCI.5127-10.2011

Carter, A.G., and W.G. Regehr. 2002. Quantal events shape cerebellar interneuron firing. *Nat. Neurosci.* 5:1309–1318. http://dx.doi.org/10.1038/nn970

Carter, B.C., A.J. Giessel, B.L. Sabatini, and B.P. Bean. 2012. Transient sodium current at subthreshold voltages: Activation by EPSP waveforms. *Neuron.* 75:1081–1093. http://dx.doi.org/10.1016/j.neuron.2012.08.033

Chavas, J., and A. Marty. 2003. Coexistence of excitatory and inhibitory GABA synapses in the cerebellar interneuron network. *J. Neurosci.* 23:2019–2031.

Christie, J.M., D.N. Chiu, and C.E. Jahr. 2011. Ca^{2+}-dependent enhancement of release by subthreshold somatic depolarization. *Nat. Neurosci.* 14:62–68. http://dx.doi.org/10.1038/nn.2718

Debanne, D., A. Bialowas, and S. Rama. 2013. What are the mechanisms for analogue and digital signalling in the brain? *Nat. Rev. Neurosci.* 14:63–69. http://dx.doi.org/10.1038/nrn3361

Dellal, S.S., R. Luo, and T.S. Otis. 2012. GABAA receptors increase excitability and conduction velocity of cerebellar parallel fiber axons. *J. Neurophysiol.* 107:2958–2970. http://dx.doi.org/10.1152/jn.01028.2011

Dudel, J., and S.W. Kuffler. 1961. Presynaptic inhibition at the crayfish neuromuscular junction. *J. Physiol.* 155:543–562. http://dx.doi.org/10.1113/jphysiol.1961.sp006646

Eccles, J.C., R.F. Schmidt, and W.D. Willis. 1962. Presynaptic inhibition of the spinal monosynaptic reflex pathway. *J. Physiol.* 161:282–297. http://dx.doi.org/10.1113/jphysiol.1962.sp006886

Fogarty, M.J., L.A. Hammond, R. Kanjhan, M.C. Bellingham, and P.G. Noakes. 2013. A method for the three-dimensional reconstruction of Neurobiotin™-filled neurons and the location of their synaptic inputs. *Front. Neural Circuits.* 7:153. http://dx.doi.org/10.3389/fncir.2013.00153

Forti, L., C. Pouzat, and I. Llano. 2000. Action potential-evoked Ca^{2+} signals and calcium channels in axons of developing rat cerebellar interneurones. *J. Physiol.* 527:33–48. http://dx.doi.org/10.1111/j.1469-7793.2000.00033.x

Glickfeld, L.L., J.D. Roberts, P. Somogyi, and M. Scanziani. 2009. Interneurons hyperpolarize pyramidal cells along their entire somatodendritic axis. *Nat. Neurosci.* 12:21–23. http://dx.doi.org/10.1038/nn.2230

Glitsch, M., and A. Marty. 1999. Presynaptic effects of NMDA in cerebellar Purkinje cells and interneurons. *J. Neurosci.* 19:511–519.

Harris, K.M., and J.K. Stevens. 1988. Dendritic spines of rat cerebellar Purkinje cells: Serial electron microscopy with reference to their biophysical characteristics. *J. Neurosci.* 8:4455–4469.

Hines, M.L., and N.T. Carnevale. 1997. The NEURON simulation environment. *Neural Comput.* 9:1179–1209. http://dx.doi.org/10.1162/neco.1997.9.6.1179

Huang, H., and L.O. Trussell. 2008. Control of presynaptic function by a persistent Na^+ current. *Neuron.* 60:975–979. http://dx.doi.org/10.1016/j.neuron.2008.10.052

Kaplan, J.H., and G.C. Ellis-Davies. 1988. Photolabile chelators for the rapid photorelease of divalent cations. *Proc. Natl. Acad. Sci. USA.* 85:6571–6575. http://dx.doi.org/10.1073/pnas.85.17.6571

Khirug, S., J. Yamada, R. Afzalov, J. Voipio, L. Khiroug, and K. Kaila. 2008. GABAergic depolarization of the axon initial segment in cortical principal neurons is caused by the Na–K–2Cl cotransporter NKCC1. *J. Neurosci.* 28:4635–4639. http://dx.doi.org/10.1523/JNEUROSCI.0908-08.2008

Kullmann, D.M., A. Ruiz, D.M. Rusakov, R. Scott, A. Semyanov, and M.C. Walker. 2005. Presynaptic, extrasynaptic and axonal $GABA_A$ receptors in the CNS: where and why? *Prog. Biophys. Mol. Biol.* 87:33–46. http://dx.doi.org/10.1016/j.pbiomolbio.2004.06.003

Llano, I., and H.M. Gerschenfeld. 1993. Inhibitory synaptic currents in stellate cells of rat cerebellar slices. *J. Physiol.* 468:177–200. http://dx.doi.org/10.1113/jphysiol.1993.sp019766

Llano, I., Y.P. Tan, and C. Caputo. 1997. Spatial heterogeneity of intracellular Ca^{2+} signals in axons of basket cells from rat cerebellar slices. *J. Physiol.* 502:509–519. http://dx.doi.org/10.1111/j.1469-7793.1997.509bj.x

Mann-Metzer, P., and Y. Yarom. 2002. Jittery trains induced by synaptic-like currents in cerebellar inhibitory interneurons. *J. Neurophysiol.* 87:149–156.

Mejia-Gervacio, S., and A. Marty. 2006. Control of interneurone firing pattern by axonal autoreceptors in the juvenile rat cerebellum. *J. Physiol.* 571:43–55. http://dx.doi.org/10.1113/jphysiol.2005.101675

Mejia-Gervacio, S., T. Collin, C. Pouzat, Y.P. Tan, I. Llano, and A. Marty. 2007. Axonal speeding: Shaping synaptic potentials in small neurons by the axonal membrane compartment. *Neuron.* 53:843–855. http://dx.doi.org/10.1016/j.neuron.2007.02.023

Midtgaard, J. 1992. Stellate cell inhibition of Purkinje cells in the turtle cerebellum in vitro. *J. Physiol.* 457:355–367. http://dx.doi.org/10.1113/jphysiol.1992.sp019382

Nusser, Z., S. Cull-Candy, and M. Farrant. 1997. Differences in synaptic GABA(A) receptor number underlie variation in GABA mini amplitude. *Neuron.* 19:697–709. http://dx.doi.org/10.1016/S0896-6273(00)80382-7

Paradiso, K., and L.-G. Wu. 2009. Small voltage changes at nerve terminals travel up axons to affect action potential initiation. *Nat. Neurosci.* 12:541–543. http://dx.doi.org/10.1038/nn.2301

Peng, H., Z. Ruan, F. Long, J.H. Simpson, and E.W. Myers. 2010. V3D enables real-time 3D visualization and quantitative analysis of large-scale biological image data sets. *Nat. Biotechnol.* 28:348–353. http://dx.doi.org/10.1038/nbt.1612

Pouzat, C., and S. Hestrin. 1997. Developmental regulation of basket/stellate cell→Purkinje cell synapses in the cerebellum. *J. Neurosci.* 17:9104–9112.

Pouzat, C., and A. Marty. 1998. Autaptic inhibitory currents recorded from interneurones in rat cerebellar slices. *J. Physiol.* 509:777–783. http://dx.doi.org/10.1111/j.1469-7793.1998.777bm.x

Pouzat, C., and A. Marty. 1999. Somatic recording of GABAergic autoreceptor current in cerebellar stellate and basket cells. *J. Neurosci.* 19:1675–1690.

Price, G.D., and L.O. Trussell. 2006. Estimate of the chloride concentration in a central glutamatergic terminal: A gramicidin perforated-patch study on the calyx of Held. *J. Neurosci.* 26:11432–11436. http://dx.doi.org/10.1523/JNEUROSCI.1660-06.2006

Pugh, J.R., and C.E. Jahr. 2011. Axonal GABAA receptors increase cerebellar granule cell excitability and synaptic activity. *J. Neurosci.* 31:565–574. http://dx.doi.org/10.1523/JNEUROSCI.4506-10.2011

Pugh, J.R., and C.E. Jahr. 2013. Activation of axonal receptors by GABA spillover increases somatic firing. *J. Neurosci.* 33:16924–16929. http://dx.doi.org/10.1523/JNEUROSCI.2796-13.2013

Pulido, C., F.F. Trigo, I. Llano, and A. Marty. 2015. Vesicular release statistics and unitary postsynaptic current at single GABAergic synapses. *Neuron.* 85:159–172. http://dx.doi.org/10.1016/j.neuron.2014.12.006

Rall, W. 1967. Distinguishing theoretical synaptic potentials computed for different soma-dendritic distributions of synaptic input. *J. Neurophysiol.* 30:1138–1168.

Rowan, M.J.M., E. Tranquil, and J.M. Christie. 2014. Distinct Kv channel subtypes contribute to differences in spike signaling properties in the axon initial segment and presynaptic boutons of cerebellar interneurons. *J. Neurosci.* 34:6611–6623. http://dx.doi.org/10.1523/JNEUROSCI.4208-13.2014

Ruiz, A.J., and D.M. Kullmann. 2012. Ionotropic receptors at hippocampal mossy fibers: roles in axonal excitability, synaptic transmission, and plasticity. *Front. Neural Circuits.* 6:112.

Ruiz, A., E. Campanac, R.S. Scott, D.A. Rusakov, and D.M. Kullmann. 2010. Presynaptic GABAA receptors enhance transmission and LTP induction at hippocampal mossy fiber synapses. *Nat. Neurosci.* 13:431–438. http://dx.doi.org/10.1038/nn.2512

Schikorski, T., and C.F. Stevens. 1997. Quantitative ultrastructural analysis of hippocampal excitatory synapses. *J. Neurosci.* 17:5858–5867.

Shu, Y., A. Hasenstaub, A. Duque, Y. Yu, and D.A. McCormick. 2006. Modulation of intracortical synaptic potentials by presynaptic somatic membrane potential. *Nature.* 441:761–765. http://dx.doi.org/10.1038/nature04720

Stell, B.M., P. Rostaing, A. Triller, and A. Marty. 2007. Activation of presynaptic GABA(A) receptors induces glutamate release from parallel fiber synapses. *J. Neurosci.* 27:9022–9031. http://dx.doi.org/10.1523/JNEUROSCI.1954-07.2007

Szabadics, J., C. Varga, G. Molnár, S. Oláh, P. Barzó, and G. Tamás. 2006. Excitatory effect of GABAergic axo-axonic cells in cortical microcircuits. *Science.* 311:233–235. http://dx.doi.org/10.1126/science.1121325

Trigo, F.F., M. Chat, and A. Marty. 2007. Enhancement of GABA release through endogenous activation of axonal GABA(A) receptors in juvenile cerebellum. *J. Neurosci.* 27:12452–12463. http://dx.doi.org/10.1523/JNEUROSCI.3413-07.2007

Trigo, F.F., A. Marty, and B.M. Stell. 2008. Axonal GABAA receptors. *Eur. J. Neurosci.* 28:841–848. http://dx.doi.org/10.1111/j.1460-9568.2008.06404.x

Trigo, F.F., J.E.T. Corrie, and D. Ogden. 2009a. Laser photolysis of caged compounds at 405 nm: Photochemical advantages, localisation, phototoxicity and methods for calibration. *J. Neurosci. Methods.* 180:9–21. http://dx.doi.org/10.1016/j.jneumeth.2009.01.032

Trigo, F.F., G. Papageorgiou, J.E.T. Corrie, and D. Ogden. 2009b. Laser photolysis of DPNI-GABA, a tool for investigating the properties and distribution of GABA receptors and for silencing neurons in situ. *J. Neurosci. Methods.* 181:159–169. http://dx.doi.org/10.1016/j.jneumeth.2009.04.022

Trigo, F.F., B. Bouhours, P. Rostaing, G. Papageorgiou, J.E.T. Corrie, A. Triller, D. Ogden, and A. Marty. 2010. Presynaptic miniature GABAergic currents in developing interneurons. *Neuron.* 66:235–247. http://dx.doi.org/10.1016/j.neuron.2010.03.030

Trigo, F.F., T. Sakaba, D. Ogden, and A. Marty. 2012. Readily releasable pool of synaptic vesicles measured at single synaptic contacts. *Proc. Natl. Acad. Sci. USA.* 109:18138–18143. http://dx.doi.org/10.1073/pnas.1209798109

Wang, D.D., and A.R. Kriegstein. 2009. Defining the role of GABA in cortical development. *J. Physiol.* 587:1873–1879. http://dx.doi.org/10.1113/jphysiol.2008.167635

Zhang, S.J., and M.B. Jackson. 1995. GABAA receptor activation and the excitability of nerve terminals in the rat posterior pituitary. *J. Physiol.* 483:583–595. http://dx.doi.org/10.1113/jphysiol.1995.sp020608